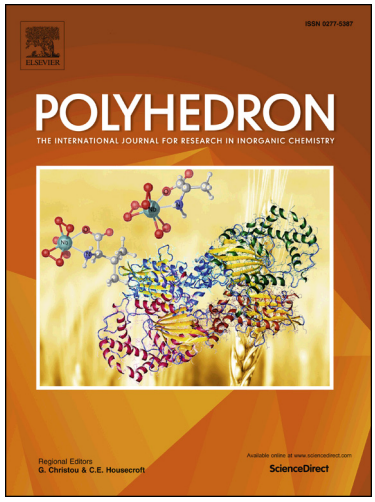

Synthesis and structural characterization of arene d^6 metal complexes of sulfonohydrazone and triazolo ligands: high potency of triazolo derivatives towards DNA binding

Lathewdeipor Shadap, Nidhi Joshi, Krishna Mohan Poluri, Mohan Rao Kollipara, Werner Kaminsky

PII: S0277-5387(18)30519-9
DOI: https://doi.org/10.1016/j.poly.2018.08.051
Reference: POLY 13374

To appear in: *Polyhedron*

Received Date: 5 July 2018
Revised Date: 17 August 2018
Accepted Date: 20 August 2018

Please cite this article as: L. Shadap, N. Joshi, K.M. Poluri, M.R. Kollipara, W. Kaminsky, Synthesis and structural characterization of arene d^6 metal complexes of sulfonohydrazone and triazolo ligands: high potency of triazolo derivatives towards DNA binding, *Polyhedron* (2018), doi: https://doi.org/10.1016/j.poly.2018.08.051

Synthesis and structural characterization of arene d^6 metal complexes of sulfonohydrazone and triazolo ligands: high potency of triazolo derivatives towards DNA binding

Lathewdeipor Shadap[a], Nidhi Joshi[b], Krishna Mohan Poluri[b], Mohan Rao Kollipara[a*], Werner Kaminsky[c]

[a]Centre for Advanced Studies in Chemistry, North-Eastern Hill University, Shillong 793 022, India. E-mail: mohanrao59@gmail.com

[b]Department of Biotechnology and Centre for Nanotechnology, Indian Institute of Technology Roorkee, Roorkee- 247 667, India.

[c]Department of Chemistry, University of Washington, Seattle, WA 98195, USA

Graphical Abstract

Reaction of 4-methyl benzenesulfonohydrazone ligands (**L1** and **L3**) with metal precursors resulted in the formation of cationic complexes with PF_6 as the counter ion. The triazolo ligand (**L2**) with metal precursor resulted in the formation of neutral complexes.

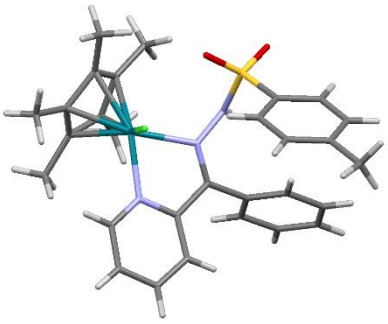

ORTEP view of Complex **2**

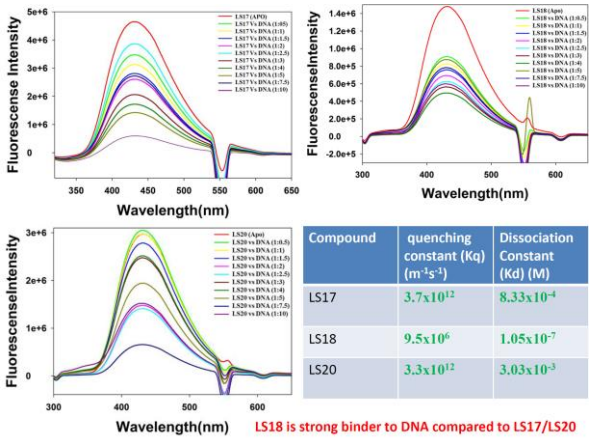

Compound	quenching constant (Kq) ($m^{-1}s^{-1}$)	Dissociation Constant (Kd) (M)
LS17	$3.7x10^{12}$	$8.33x10^{-4}$
LS18	$9.5x10^{6}$	$1.05x10^{-7}$
LS20	$3.3x10^{12}$	$3.03x10^{-3}$

LS18 is strong binder to DNA compared to LS17/LS20

Abstract

Complexation of [(*p*-cymene)$RuCl_2]_2$ and [Cp*$MCl_2]_2$ (M = Rh/Ir) with chelating ligand 4-methylbenzenesulfonohydrazone ligands (**L1** and **L3**) resulted in the formation of mononuclear cationic complexes having PF_6 as the counter ion whereas, complexation with the triazolo pyridine based ligand (**L2**) resulted in neutral complexes with mono-dentate binding fashion to the metal center. All these complexes were fully characterized by analytical, spectroscopic and X-ray diffraction studies. The complexes showed typical piano stool geometry around the metal center with the ligands acting as NN' donor chelating ligand (for **L1** and **L3**) and mono-dentate ligand (for **L2**). Biological studies such as antibacterial and DNA binding studies were screened for the ligands as well as for the complexes. The complexes as well as ligands have not indicated any antibacterial activity but the triazolo ligand (**L2**) as well as complex **4** and complex **6** exhibited DNA binding activity.

Keywords: 4-methylbenzenesulfonohydrazone, triazolo, DNA binding studies, antibacterial study

1. Introduction

Half sandwich complexes of some platinum group metals (ruthenium, rhodium, iridium) containing heterocyclic nitrogen based ligands have emerged to be popular and well- studied in the field of organometallics due to their readiness to form stable complexes [1, 2], unique properties; mild reaction conditions, photochemical properties, catalytic activities, electrochemical behavior as well as biological activities such as cytotoxic, antibacterial, antimalarial activities, *etc.*, [3-10].

The heterocyclic nitrogen based ligands such as pyridine-based hydrazones and triazolo derivatives have been found to be the fundamental building blocks for numerous pharmaceutical and functional materials. In fact, the hydrazone derivatives can behave as bidentate / tridentate chelating ligands due to the presence of lone pair of electrons on the nitrogen atom which can bind to the metal center and have found their applications in coordination chemistry, florescence sensors and chemosensors chemistry, showing catalytic properties and behaving as pharmaceutical active agents [11-14]. Biologically, hydrazones show a wide range of biological activities such as cytotoxicity, antitumor, antimicrobial, and anti-inflammatory [15-19].

The properties of platinum group metals such as ruthenium, rhodium and iridium as well as hydrazones and environmental remediation curved our minds to synthesize and study the following reported benzenesulfonohydrazone ligand complexes with *p*-cymene ruthenium, Cp* rhodium and Cp* iridium to further explore the coordination of the hydrazone derivative ligands to the metal as well as to investigate the biological activity of the complexes.

In our path to synthesize the reported hydrazone ligands according to the reported procedure [20, 21], we were not only able to synthesize our desired ligands **L1** and **L3** (Scheme **1** and **3**) but unexpectedly, ligand **L2** (which is a triazolo derivative ligand) was also obtained which had resulted from the side product of ligand **L1** (Scheme **1**).

Triazolopyridines derivatives are an important class of compounds and have been widely explored by Jones *et al.* [22] and Abarca *et al.* [23], since the early 1980s. Traditionally, triazolo pyridine based derivatives have been synthesized by oxidative cyclization of 2- pyridyl ketone hydrazones by using at least a stoichiometric of oxidants such as copper salts which have shown to be more effective in providing appropriate yield. Other oxidants may include Ag_2O, MnO_2, hypervalent iodine and Ni peroxide [24-28].

The formation of ligand **L2** provides an alternative route to the synthesis of triazolo pyridine based ligands by decomposition of the hydrazones. This has also occurred in the case of dipyridyl ketone, which in this case resulted in the formation a bidentate chelating triazolo ligand [29]. Compounds containing triazolo moiety have been found to be highly interesting due to readiness to complex with heavy metals, cationic, neutral or anionic species of biomedical or environmental relevance. They can also show interesting magnetic properties as well as fluorescent properties [30].

With such properties possessed by the hydrazone as well as the triazolo ligands, we are determined to explore the coordination of the complexes of these ligands with the platinum group metal precursors of ruthenium, rhodium and iridium as well as to investigate their biological activities.

As far as our knowledge is concern, no other work as such has been reported to carry out the synthesis and studies of metal complexes **1-9** comprising of the ligands **L1**, **L2** and **L3** for which the ligands have been prepared according to the reported procedure [20, 21].

2. Experimental

2.1 Materials and methods

2-Acetylpyridine and 2-benzoylpyridine were purchased from Aldrich and used as such without further purification; the solvents were purified and dried according to standard procedures [31].

The starting precursor metal complexes [(*p*-cymene)$RuCl_2]_2$ and [Cp*$MCl_2]_2$ (M = Rh/Ir) were prepared according to the reported literature [32, 33]. Ligands (**L1** and **L3**) were prepared according to the reported procedures [21] whereas the formation of triazolo ligand **L2** was unexpected. During the course of preparation of ligand **L1** following the reported procedure, two distinct spots and one spot (unreacted reactant) were observed at the bottom by TLC. The upper spot corresponds to ligand **L1** which precipitates out as orange crystalline solids out of the reaction mixture on cooling, while the lower spot corresponds to ligand **L2** which was obtained after passing through column as creamy white solids. The ligands (**L1** and **L2**) were washed with diethyl ether and air-dried.

2.2 Single crystal X-ray diffraction

Crystal's suitable for X-ray analyses for complexes **2**, **3**, **4**, **6**, **7**, **8**, and **9** were obtained by slow diffusion of hexane/diethyl ether into DCM/$CHCl_3$ solution and their molecular structures have been given in Figure 1-3 while for complex **9,** the ORTEP view has been given just to show the mode of binding and the composition of the metal complex due to low theta value. The single crystals of complexes were attached to a glass fiber and placed into the Oxford Diffraction Xcalibur Eos Gemini diffractometer. Single crystal X-ray diffraction data for the complexes were collected on an Oxford Diffraction Xcalibur Eos Gemini diffractometer using graphite monochromatic Mo-Kα radiation (λ = 0.71073 Å). The strategy for the data collection was evaluated using the CrysAlisPro CCD software [34]. Crystal data were collected by standard ''phi–omega scan'' techniques and were scaled and reduced using CrysAlisPro RED software. The structures were solved using SHELX and refined by full-matrix least squares with SHELX refining on F^2 [35, 36]. The metal atoms in the complex were located from the E-maps and non-hydrogen atoms were refined anisotropically. The hydrogen atoms bound to the carbon were placed in geometrically constrained positions and refined with isotropic temperature factors, generally 1.2 or 1.5 U_{eq} of their parent atoms. The crystallographic and structure refinement parameters for the complexes are listed in Table 1 and 2, and selected bond lengths and bond

angles are presented in Table 3 and 4. The molecular structures were drawn with ORTEP3 program [37] whereas packing pattern and interactions like H- bonding, π---π, *etc*, were drawn using MERCURY [38].

2.3. In-vitro antibacterial studies: The bactericidal efficacy of the synthesized compounds was evaluated by agar well diffusion method as described elsewhere. Each well diffusion experiment was performed in triplicate with 1 mg mL^{-1} concentration of complexes. Dimethylsulphoxide (DMSO) was used as a solvent and as a negative control, whereas gentamycin antibiotic was used as positive control.

2.4. Fluorescence studies on DNA interaction: Experiments involving the interaction of complexes with SM-DNA (SM - Salmon milt) were carried-out in 5 mM Tris–HCl and 50 mM NaCl buffer of pH 7.4. The concentration of SM-DNA per nucleotide was determined by absorption spectroscopy at 260 nm. All florescence titration experiments were carried out with fixed concentration (20 µM) of ligand (**L2**), complex **4** and complex **6** while gradually increasing the DNA concentration (10 µM - 200 µM). For all complexes, emission spectra were recorded at 300-650 nm by exciting them at 275 nm. Complexes were incubated for 15 min at room temperature to achieve thermodynamic equilibrium before spectral recording. Experiments were repeated twice for reproducibility. To elucidate this quenching phenomenon, the quenching data were analyzed with Stern–Volmer equation.

$$F_0/F = 1+K_q\tau_0\,[Q] = 1 + K_{SV}\,[Q] \quad \ldots\ldots\ldots\ldots\ldots\ldots (1)$$

Where F_0 and F represent the fluorescence intensities in the absence and in the presence of quencher, K_q is the quenching rate constant of the bimolecular, K_{SV} is the dynamic quenching constant, τ_0 is the average lifetime of the molecule without quencher and [Q] is the concentration of the quencher.

Furthermore, the relationship between fluorescence quenching intensity and the concentration of quenchers can be described by the binding constant equation (2).

$$\log [F0-F/F] = \log Ka + n \log [Q] \ldots\ldots\ldots\ldots\ldots (2)$$

From this equation, a double logarithm plot can be obtained which gives us the necessary binding / dissociation constants.

2.5. General procedure for synthesis of mononuclear ruthenium complexes of L1, L2 and L3

Metal precursor [(*p*-cymene)$RuCl_2]_2$ (0.1 mmol), ligands (**L1**, **L2** and **L3**) (0.2 mmol) and 3mmol of NH_4PF_6 were dissolved in dry methanol (10 mL) and stirred for about 4 hours at room temperature. After 1 hour, a yellowish-orange precipitate appeared in the reaction mixture. The precipitate was filtered, washed with cold methanol (2×5 mL) and then with diethyl ether (3×5 mL) and was air- dried.

2.5.1. [(p-cymene)Ru(L1)Cl]PF_6 (1)

Yield (76%); Orange; IR (KBr, cm^{-1}): 3447 $\nu_{(N-H)}$, 1597 $\nu_{(C=N)}$, 1469 $\nu_{(N-H)bending}$, 1350 $\nu_{(S=O)asym}$ and 1307 $\nu_{(S=O)asym}$, 1232 $\nu_{(C-N)}$, 1150 $\nu_{(S=O)sym}$, 871 $\nu_{(P-F)}$, 768 $\nu_{(S-N)}$, 674 $\nu_{(N-H)wagging}$; ^{1}H NMR (400 MHz, $CDCl_3$): δ = 9.28 (d, 1H, *J* = 8Hz), 7.85 (d, 2H, *J* = 12Hz), 7.58(t, 1H, *J* = 8Hz), 7.30 (t, 3H, *J* = 4Hz), 7.2-7.13 (m, 7H), 5.85 (d, 1H, *J* = 4Hz, $CH_{(p\text{-}cym)}$), 5.69 (d, 2H, *J* = 4Hz, $CH_{(p\text{-}cym)}$), 5.67 (d, 1H, *J* = 8Hz, $CH_{(p\text{-}cym)}$), 5.55 (d, 1H, *J* = 8Hz), 2.84 (sept, 1H, $CH_{(p\text{-}cym)}$), 2.35(s, 3H), 2.31 (s, 3H, $CH_{(p\text{-}cym)}$), 1.25(d, 3H, *J* = 8Hz, $CH_{(p\text{-}cym)}$), 1.15 (d, 3H, *J* = 4Hz, $CH_{(p\text{-}cym)}$); Mass- ESI (m/z): 586.14 $[M\text{-}PF_6\text{-}Cl]^{2+}$; UV–Vis {Acetonitrile, λ_{max}, nm ($\varepsilon/10^{-4}$ M^{-1} cm^{-1})}: 235 (3.413), 264 (2.133), 309 (1.277), 408 (0.327).

2.5.2. [(p-cymene)Ru(L2)Cl_2 (4)

Yield (72%); Reddish orange; IR (KBr, cm^{-1}): 1632 $\nu_{(C=C)}$, 1606 $\nu_{(C=C)}$, 1494 $\nu_{(C=N)}$, 1471 $\nu_{(C=C)}$, 1454 $\nu_{(C=C)}$, 1432 $\nu_{(N=N)}$, 1224 $\nu_{(C-N)}$; ^{1}H NMR (400 MHz, $CDCl_3$): δ = 8.79 (d, 1H, *J* = 8Hz), 8.04 (d, 1H, *J* = 8Hz), 7.97 (d, 2H, *J* = 4Hz), 7.53 (t, 2H, *J* = 8Hz), 7.42- 7.40 (m, 1H), 7.35(d, 1H, *J* = 8Hz), 7.06 (t, 1H, *J* = 8Hz), 5.67 (d, 2H, *J* = 8Hz,), 5.60 (d, 2H, *J* = 8Hz), 3.04 (sept, 1H, $CH_{(p\text{-}cym)}$), 2.28 (s, 3H, $CH_{(p\text{-}cym)}$), 1.31 (d, 6H, *J* = 8Hz, $CH_{(p\text{-}cym)}$); Mass- ESI (m/z): 270.91 [M-

triazole-Cl]$^{2+}$; UV–Vis {Acetonitrile, λ_{max}, nm ($\varepsilon/10^{-4}$ M^{-1} cm^{-1})}: 218 (4.399), 272 (4.201), 330 (1.126), 405 (0.114).

2.5.3. [(p-cymene)Ru(L3)Cl]PF_6 (7)

Yield (80%); Red; IR (KBr, cm^{-1}): 3437 $\nu_{(N-H)}$, 1573 $\nu_{(C=N)}$, 1452 $\nu_{(N-H)bending}$, 1357 $\nu_{(S=O)asym}$ and 1302 $\nu_{(S=O)sym}$, 1239 $\nu_{(C-N)}$, 1159 $\nu_{(S=O)sym}$, 842 $\nu_{(P-F)}$, 778$\nu_{(S-N)}$, 684 $\nu_{(N-H)wagging}$; ^{1}H NMR (400 MHz, $CDCl_3$): δ = 7.50 (d, 1H, *J* = 4Hz), 8.23 (d, 2H, *J* = 4Hz), 7.94 (d, 3H *J* = 8Hz), 7.81- 7.77 (m, 1H,), 7.42 (d, 2H, *J* = 8Hz), 6.14 (d, 2H, *J* = 4Hz), 5.73 (d, 1H, *J* = 4Hz, $CH_{(p\text{-cym})}$), 5.64 (d, 1H, *J* = 4 Hz, $CH_{(p\text{-cym})}$), 2.65 (sept, 1H, $CH_{(p\text{-cym})}$), 2.47 (s,3H), 2.36 (s,3H, $CH_{(p\text{-cym})}$), 2.16 (s, 3H,) 1.00 (d, 3H, *J* = 8Hz, $CH_{(p\text{-cym})}$), 0.94 (d, 3H, *J* = 8 Hz, $CH_{(p\text{-cym})}$); Mass- ESI (m/z): 562.04 [M-PF_6+2H]$^+$; UV–Vis {Acetonitrile, λ_{max}, nm ($\varepsilon/10^{-4}$ M^{-1} cm^{-1})}: 227 (5.203), 278 (2.075), 337 (0.617), 408 (0.544).

*2.6. General procedure for preparation of mononuclear Cp*Rh and Cp*Ir complexes of L1, L2 and L3*

Metal precursor [Cp*MCl_2]$_2$ (M = Rh/Ir) (0.1 mmol), ligands (**L1**, **L2**, **L3**) (0.2 mmol) and 3 equivalents of NH_4PF_6 were dissolved in dry methanol (10 mL) and stirred at room temperature for 4 hours. After 1-2 hours a yellow/orange compound precipitated out from the reaction mixture. The precipitate was filtered, washed with cold methanol (2 x 5 mL) and diethyl ether (3 x 10 mL) and air-dried.

*2.6.1. [Cp*Rh(L1)Cl]PF_6 (2)*

Yield (82%); Orange; IR (KBr, cm^{-1}): 3441 $\nu_{(N-H)}$, 1583 $\nu_{(C=N)}$, 1461$\nu_{(N-H)bending}$, 1360 $\nu_{(S=O)asym}$ and 1305 $\nu_{(S=O)asym}$, 1231 $\nu_{(C-N)}$, 1169 $\nu_{(S=O)sym}$, 871 $\nu_{(P-F)}$, 764 $\nu_{(S-N)}$, 671 $\nu_{(N-H)wagging}$; ^{1}H NMR (400 MHz, $CDCl_3$): δ = 8.87 (d, 1H, *J* = 4Hz), 8.01 (t, 1H, *J* = 4Hz), 7.88- 7.82 (m, 3H), 7.72 (t, 1H, *J* = 4Hz), 7.57 (t, 3H, *J* = 8Hz), 7.43 (s, broad, 1H), 7.33 (d, 2H, *J* = 4Hz), 7.07 (t, 2H, *J* = 4Hz), 2.74 (s, 3H,), 1.75 (s, 15H, $CH_{(Cp^*)}$); Mass- ESI (m/z): 623.99 [M-PF_6-2H] and 588.07 [M-PF_6-Cl-2H]$^{2+}$; UV–Vis {Acetonitrile, λ_{max}, nm ($\varepsilon/10^{-4}$ M^{-1} cm^{-1})}: 229 (6.695), 278 (2.429), 389 (0.754).

*2.6.2. [Cp*Rh(L2)Cl_2] (5)*

Yield (77%); Orange; IR (KBr, cm^{-1}): 1633 $\nu_{(C=C)}$, 1610 $\nu_{(C=C)}$, 1541 $\nu_{(C=N)}$, 1458 $\nu_{(C=C)}$, 1414 $\nu_{C=C)}$, 1327 $\nu_{(N=N)}$, 1230 $\nu_{(C-N)}$; ^{1}H NMR (400 MHz, $CDCl_3$ + DMSO): δ = 8.86 (d, 1H, *J* = 8Hz), 8.09 (d, 1H, *J* = 8Hz), 7.96 (d, 1H, *J* = 8Hz), 7.72 (s,1H), 7.53 (t, 2H, *J* = 8Hz), 7.44- 7.38 (m, 2H), 7.13 (t, 1H, *J* = 4Hz), 1.75 (s, 15H, $CH_{(Cp^*)}$); Mass- ESI (m/z): 274.89 $[M\text{-triazole-Cl}]^+$; UV–Vis {Acetonitrile, λ_{max}, nm ($\varepsilon/10^{-4}$ M^{-1} cm^{-1})}: 231(3.808), 266 (1.547), 406 (0.613).

*2.6.3. [Cp*Rh(L3)Cl]PF_6 (8)*

Yield (77%); Orange; IR (KBr, cm^{-1}): 3412 $\nu_{(N-H)}$, 1599 $\nu_{(C=N)}$, 1459 $\nu_{(N-H)bending}$, 1350 $\nu_{(S=O)asym}$, 1218 $\nu_{(C-N)}$, 1170 $\nu_{(S=O)sym}$, 849 $\nu_{(P-F)}$, 777 $\nu_{(S-N)}$, 679 $\nu_{(N-H)wagging}$; ^{1}H NMR (400 MHz, $CDCl_3$): δ = 8.96 (d, 1H, *J* = 4Hz), 8.16 (t, 1H, *J* = 8Hz), 8.05 (d, 1H, *J* = 8Hz), 7.92 (d, 2H, *J* = 8Hz), 7.85 (t, 1H, *J* = 8Hz), 7.23 (d, 3H, *J* = 8Hz), 2.27 (s, 3H), 2.06(s, 3H) 1.67 (s, 15H, $CH_{(Cp^*)}$); Mass- ESI (m/z): 561.99 $[M\text{-}PF_6\text{-}2H]^+$ and 526.06 $[M\text{-}PF_6\text{-Cl-}2H]^{2+}$; UV–Vis {Acetonitrile, λ_{max}, nm ($\varepsilon/10^{-4}$ M^{-1} cm^{-1})}:227 (5.793), 278 (3.163), 376 (0.487), 386 (0.462).

*2.6.4. [Cp*Ir(L1)Cl]PF_6 (3)*

Yield (70%); Yellowish orange; IR (KBr, cm^{-1}): 3446 $\nu_{(N-H)}$, 1582 $\nu_{(C=N)}$, 1450 $\nu_{(N-H)bending}$, 1359 $\nu_{(S=O)asym}$, 1309 $\nu_{(S=O)sym}$, 1159 $\nu_{(S=O)sym}$, 868 $\nu_{(P-F)}$, 761 $\nu_{(S-N)}$, 672 $\nu_{(N-H)wagging}$; ^{1}H NMR (400 MHz, $CDCl_3$): δ = 8.90 (d, 1H, *J* = 8Hz), 7.87 (d, 2H, *J* = 8Hz), 7.67- 7.60 (m, 1H), 7.36- 7.31 (m, 3H), 7.28 (m, 3H), 7.21 (d, 2H, *J* = 8Hz), 7.16 (d, 2H, *J* = 8 Hz), 2.33 (s, 3H), 1.66 (s, 15H, $CH_{(Cp^*)}$); Mass- ESI (m/z): 714.07 $[M\text{-}PF_6\text{-}H]^+$and 678.15 $[M\text{-}PF_6\text{-Cl+}H]^{2+}$; UV–Vis {Acetonitrile, λ_{max}, nm ($\varepsilon/10^{-4}$ M^{-1} cm^{-1})}: 223 (5.420), 265 (2.682), 429 (0.503).

*2.6.5. [Cp*Ir(L2)Cl_2 (6)*

Yield (78%); yellow; IR (KBr, cm^{-1}): 1621 $\nu_{(C=C)}$, 1609 $\nu_{(C=C)}$, 1542 $\nu_{(C=N)}$, 1479 $\nu_{(C=C)}$, 1434 $\nu_{(C=C)}$, 1422 $\nu_{(N=N)}$, 1217 $\nu_{(C-N)}$; ^{1}H NMR (400 MHz, $CDCl_3$): δ = 8.00 (d, 1H, *J* = 8Hz), 7.91 (d, 2H, *J* = 8Hz), 7.55 (t, 3H, *J* = 8Hz), 7.44 (t, 1H, *J* = 8Hz), 7.37 (t, 1H, *J* = 4Hz), 7.04 (t, 1H, *J* = 8Hz), 1.63 (s, 15H, $CH_{(Cp^*)}$); Mass- ESI (m/z): 522.13 $[M\text{-}2HCl]^{2+}$ and 362.98 [M-triazole+2H-

Cl]$^{+}$; UV–Vis {Acetonitrile, ν λ_{max}, nm ($\varepsilon/10^{-4}$ M^{-1} cm^{-1})}: 218 (3.821), 261 (1.698), 331 (1.219), 409 (0.166).

*2.6.6. [Cp*Ir(L3)Cl]PF_6 (9)*

Yield (74%); Yellow; IR (KBr, cm^{-1}): 3422 $\nu_{(N-H)}$, 1598 $\nu_{(C=N)}$, 1459 $\nu_{(N-H)bending}$, 1351 $\nu_{(S=O)asym}$, 1171 $\nu_{(S=O)sym}$, 851$\nu_{(P-F)}$, 778 $\nu_{(S-N)}$, 667 $\nu_{(N-H)wagging}$; ^{1}H NMR (400 MHz, $CDCl_3$): δ = 8.63 (d, 1H, *J* = 4Hz), 8.04 (t, 1H, *J* = 8Hz), 7.94 (d, 2H, *J* = 8Hz), 7.90 (d, 1H, *J* = 8Hz), 7.73 (t, 1H, *J* = 8Hz), 7.29- 7.26 (m, 3H,), 2.41 (s, 3H), 2.03(s, 3H) 1.74 (s, 15H, $CH_{(Cp^*)}$); Mass- ESI (m/z):652.14 [M-PF_6-H]$^{+}$; UV–Vis {Acetonitrile, λ_{max}, nm ($\varepsilon/10^{-4}$ M^{-1} cm^{-1})}: 228 (6.632), 277 (3.812), 383 (0.768).

3. Results and discussion

3.1. Synthesis of the complexes

The reaction of metal precursors with benzenesulfonohydrazone ligands (**L1** and **L3**) with appropriate ratio in dry methanol resulted in the formation of mononuclear complexes. In the formed complexes with ligand **L1** and **L3**, the ligands act as bidentate NN' chelating ligands whereas the reaction of metal precursors with the unexpected formed triazolo ligand (**L2**) resulted in the formation of neutral complexes with the ligand acting as a mono-dentate ligand Scheme 3. The molecular structures of the complexes (**2**, **3**, **4**, **6**, **7**, **8**, **9**) were determined by single crystal X-ray analysis. Complexes (**2**, **3**, **7**, **8**, **9**) were isolated as cationic complexes with PF_6 as the counter ion whereas complexes (**4** and **6**) were isolated as neutral complexes. The ORTEP view of complex **9** has been given just to show the mode of binding and the composition of the metal complex due to low theta value. All the complexes were isolated as yellow to orange solids and were found to be stable in air and non- hygroscopic. These complexes are soluble in acetonitrile, dichloromethane, DMSO, chloroform but insoluble in hexane, diethyl ether and pet ether.

3.2. Spectral studies of the complexes

Information about the ligands and the complexes has been studied by IR spectra, which revealed significant information. Stretching frequencies of NH is observed around 3412 - 3447 cm^{-1} indicating that there is no bonding to the metal atom. The stretching frequency of S=O in free ligands is around in the range 1225 - 980 cm^{-1} whereas in the complexes, we observed symmetric as well as asymmetric stretching; the symmetric stretching frequency $\upsilon_{(S=O)sym}$ is observed in the range 1360 - 1350 cm^{-1} and the asymmetric stretching frequency $\upsilon_{(S=O)\ asym}$ is observed in the range 1171-1150 cm^{-1} indicating that there is no bonding through oxygen atom to the metal center. In case of ligand (**L2**), the stretching frequency of S=O is absent which indicates the dissociation of the sulfonyl group resulting in the formation of the triazolo ligand. Similarly, in complexes **4, 5** and **6** the stretching frequency of S=O is absent. The C=N stretching frequency for the ligands lies in the range of 1600-1650 cm^{-1} while for the complexes, the C=N stretching frequency is observed in the range 1599-1573 cm^{-1}. This decrease in the stretching frequency of C=N indicates the binding of nitrogen to the metal atom. In all the complexes except for complexes **4, 5** and **6**, the presence of the counter ion PF_6 has been observed in the range 871 - 842 cm^{-1} due to P-F stretching frequency [40]. The stretching frequency of aromatic C=C has been observed in the range 1640- 1600 cm^{-1} and 1494- 1414 cm^{-1} while that of N=N has been observed in the range 1432-1327 cm^{-1}.

^{1}H NMR studies of the complexes

The ^{1}H NMR spectra of the complexes have been provided in the supplementary information (Figure S1-S10). To confirm the formation of the complexes have been confirmed through NMR studies which showed the appearance of the ligand proton signals as well as *p*-cymene and Cp* ring protons. The aromatic protons of the ligands can be observed in the downfield region between 7.06-9.28 ppm. The N-H proton signal for all the complexes except **4, 5** and **6** has been observed to couple with the other aromatic ligand protons. For complexes **4, 5** and **6** N-H proton is absent. It has also been observed that there is an unusual splitting pattern of signal for *p*-

cymene moiety in all the three complexes (**1, 4, 7**). In complex **1**, we observe the aromatic proton signals of *p*-cymene ring splits into four doublets in the range 5.55- 5.85, while in complex **4**, we observed two doublets around 5.67 ppm and 5.60 ppm and in complex **7**, we observed three doublets in the range 5.64-6.14 ppm. In complex **4**, we observed a doublet at 1.31 ppm while in complexes **1** and **7,** we observed two doublets for the six methyl protons of *p*-cymene instead of one doublet in the range 0.95-1.25 ppm. This unusual pattern can be attributed to the diastereotopic effect of the methyl protons of the isopropyl group and the methine protons of the *p*-cymene ring as well as the chirality of the metal upon coordination with hydrazone ligands [41]. Septet signal for complexes **1, 4, 7** have been observed at 2.84 ppm, 3.04 ppm and 2.65 ppm respectively and singlet signal for methine protons of *p*-cymene have been observed at 2.31 ppm, 2.28 ppm and 2.16 ppm respectively. In rhodium and iridium complexes, in addition to the protons of the ligands, we have also observed a sharp singlet around 1.63-1.75 ppm for complexes **2**, **3**, **5**, **6**, **8**, **9** corresponding to Cp* protons. By and large, the NMR data of all the complexes are with expected resonance and integration with the formulated complexes.

Mass spectral studies of the complexes

Mass spectral data of the complexes have been provided in the supplementary data (Figure S11-S19) and their values are given in the experimental section. The analysis of these complexes were done in acetonitrile. The analyzed masses of the complexes are found to be consistent and tallied with the calculated masses. The molecular ion peaks of all the complexes are found to be in well agreement with the calculated masses. The found molecular ion peaks (for each complex) are displayed at m/z: 586.14(**1**), m/z: 588.07(**2**), m/z: 679.87 (**3**), m/z: 270.91 (**4**), m/z: 274.89(**5**), m/z: 522.13 (**6**), m/z: 560.09 (**7**), m/z: 526.06 (**8**), m/z: 652.14 (**9**). In all the cationic complexes, fragmentation of the counter ion as well as the chloride was observed while in the neutral complexes of triazole, we observed fragmentations of triazole ligand from the metal

center. The consistent molecular ion peaks of the all complexes with the calculated mass, shows that there is a strong bonding of the arene ring (arene= *p*-cymene, Cp*) to the metal atom.

UV- Visible description of metal complexes

The electronic spectra of the metal complexes were recorded in acetonitrile with 10 μM concentrations at room temperature and these spectra have been provided in the supplementary data (Figure S20). These complexes are d^6 low spin metal complexes containing filled orbitals of proper geometry at the metal centers which can interact with the low lying π * orbitals of the ligands which may result in metal- to- ligand charge transfer (MLCT) transitions [42, 43]. The low energy absorption band observed in the range 385- 408 nm is assigned to metal- to- ligand charge transition (MLCT) dπ(M) to π*(L) transitions while the high energy absorption band observed in the range 218- 235 nm and 265-331 nm may be attributed to ligand- center π- π* / n- π* transitions [44, 45].

Description of molecular structures of metal complexes

To get a deeper and broader understanding about the spatial arrangement and interactions among the molecules in a unit cell as well as the information about the coordination in metal complexes, metal complexes are crystallized; which in our case the metal complexes have been crystallized by using slow diffusion method of hexane/ diethyl ether into a saturated solution of metal complexes in DCM / $CHCl_3$. Through crystallography studies, a variety of binding modes and coordination in the metal complexes can be studied and known which other spectroscopic studies are unable to do so. In this structural analysis, we have been able to establish the crystal structures of some of the metal complexes. The ORTEP view of the isolated crystal structures (**2**, **3**, **4**, **6**, **7**, **8**, **9**) with atom numbering are presented in Figures 1-3 and the relevant crystallographic parameters along with the details of bond lengths; bond angles are listed in Table 1, 2, 3 and 4. Complex **6** crystallized along with metal precursor, which may be due to presence of excess metal precursor, which was able to stay even after washing with cold

methanol. For complex **9,** its ORTEP view has been given just to present the structure, composition and confirmation of the metal complex as the crystal has a low theta value.

Single crystals were attached to a glass fiber and transferred to the Oxford Diffraction Xcalibur Eos Gemini diffractometer. For complexes **2**, **3**, **7, 8** and **9**, X- ray studies showed that these complexes are cationic complexes bearing the general formula [(arene)M(L)Cl]PF_6. The metal complexes featured a regular three-legged " piano stool" geometry in which the arene ring (arene= *p*-cymene, Cp*) occupied the coordination sites around the metal in η^5/η^6 manner, terminal chloride and chelating N, N donor ligand. The metal atom shows pseudo octahedral geometry with the arene ring occupying the three facial geometry acting as the seat of a piano and the nitrogen donor atoms from hydrazone ligands and chloride atom acting as the three legs of a piano. The molecular structures of these complexes (**2**, **3**, **7, 8** and **9**) revealed the hydrazone derivative ligands bind to the metal in a bidentate manner through imine nitrogen and nitrogen of the pyridine ring leading to the formation of a five membered chelated ring with PF_6 as the counter ion.

In the case of complexes **4** and **6** we observed the binding of the ligand (**L2**) to metal atom takes place only through the nitrogen atom of the triazolo ligand, which resulted in the formation of mono-dentate neutral complexes. The crystallized systems of the complexes **2**, **3**, **4**, **6, 7** and **8** are given in Table **1** and **2**. The distances between the metal (M) center to the centroid of the *p*-cymene/Cp* ring of the complexes has been provided in Table **3** and **4**. For complexes **2**, **3**, **7**, and **8**, the metal to pyridyl nitrogen [M(1)-N(1)], the metal to imine nitrogen [M(1)-N(2)] and the metal to chloride [M(1)-Cl(1)] bond lengths as well as their respective bond angle values [N(1)-M(1)-N(2)], [N(1)-M(1)-Cl(1)] and [N(2)-M(1)-Cl(1)] of these complexes are given in Table **3** and are found to be comparable to the previous reported values [46, 47] . The S=O bond distances for complexes **2**, **3**, **7** and **8** are found to be in the range 1.415-1.435 Å. Similarly, in case of complexes **4** and **6**, the metal to triazolo nitrogen [M(1)-N(2)], the metal to chloride

[M(1)-Cl(1)] and [M(1)-Cl(2)] bond lengths as well as their respective bond angle values are given in Table **4**. The bond angle values of these complexes **2**, **3**, **4**, **6**, **7** and **8** are comparable to the piano stool arrangement at the metal atom and are comparable to reported values for closely related systems [48-50].

The crystal packing of these complexes shows some inter molecular hydrogen bonding such as C-H---Cl, O---H and π---π that contributes towards the stability of the complexes. Complex **2** and **3** show two types of inter hydrogen bonding *i.e* for complex **2**, O(2)---(3)H and H(29)---Cl(1) distanced at 2.325 Å and 2.905 Å respectively and for complex **3** O(2)---(3)H and H(17)---Cl(1) distanced at 2.330 Å and 2.843 Å respectively (Figure 4). In complex **4**, we observed one inter hydrogen bonding only *i.e* H(18)---Cl(2) distanced at 2.759 Å (Figure 5) which is due to the interaction of chlorine and C-H of the phenyl ring while in complex **6**, we observed two types of interactions *i.e*, inter hydrogen bonding H(14)---Cl(1) and H(22)---Cl(1) distanced at 2.863 Å and 2.868 Å respectively and C to π interaction which values at 3.589 Å (Figure 5). The H---Cl interactions in complex **6** is due to the interaction of the chlorine atom (Cl1) and hydrogen atom H(22) of the phenyl ring (2.868 Å) and chlorine atom (Cl1) with the hydrogen atom H (14) of the phenyl fused triazole ring (2.863 Å). Complex **7** shows similar inter hydrogen bonding H(17C)---O(2) distanced at 2.678 Å (Figure 6) as that of complexes **2** and **3** while in complex **8**, in addition to inter hydrogen bonding O(2)---H(3N) distanced at 2.199 Å, we also observed O(2)---N(3) interactions distanced at 2.933 Å as shown in figure 6. These types of interactions pave way for supramolecular motifs. Interestingly, in complex **9**, we observed π-π interaction at 3.988 Å (Figure 6) between the pyridyl rings leading to the formation of dimeric unit.

3.3. Biological studies on metal-ligand complexes

(i) In- vitro antibacterial assay: Due to the massive resistance of bacteria to various drugs has raised a considerable interest in developing of new classes of antimicrobial agents. Here in

present study the synthesized complexes were investigated using zone inhibition assay to exert their activity against two Gram positive bacteria *S. aureus* and *B. thuringiensis* and two Gram negative bacteria *E. coli* and *P. aeruginosa*. None of the tested complexes show any significant bactericidal activity against the tested Gram positive and Gram negative bacteria with reference to gentamycin which is used as a positive control (Figure S21).

(ii) DNA binding studies: The search for alternative drugs to the well-known anti-cancer agent Cisplatin is in progress considering the potency of the platinum group metallodrugs (51, 52). The anti-cancer action of these metallocomplexes is based on the direct binding and DNA damage (53). Hence, the binding studies between a novel transition metal-ligand complexes with DNA may pave the way for exploration and characterization that further can translate into a therapeutic lead (54, 55). In the current study the binding propensity between synthesized complexes with SM-DNA were explored by florescence spectroscopy using quenching experiments. The fluorescence spectra of synthesized complexes (**4** and **6**) and ligand (**L2**) with increasing concentration of SM-DNA were quenched remarkably and significant decrease in the emission profile intensities were observed upon adding SM-DNA indicating for a specific interaction between SM-DNA and the ligand (**L2**) and complexes (**4** and **6**) (Figure 7 A-C). Using a double logarithmic plot (Figure 7 D-F), the binding constants were calculated as discussed in the materials and methods (Table 5). The dissociation constant of ligand (**L1**) and complex **6** suggested weak binding to DNA. Amongst all, complex **4** binds strongly to DNA with a sub-micro molar affinity, thus indicating its potency to be further evaluated for in-vitro and in-vivo studies as an anti-cancer agent.

Conclusion

In summary, we have successfully synthesized the complexes of ruthenium, rhodium and iridium with hydrazones (**L1** and **L3**) and triazolo (**L2**) as ligands. All these complexes have been characterized by various spectroscopic techniques and molecular structures have been

determined by X-ray diffraction study. These complexes as well as the respective ligands, though they did not display any antibacterial activity, yet, ligand **L2**, complex **4** and complex **6** have revealed the binding to DNA for which their florescence spectra with increase in concentration of SM-DNA were quenched remarkably and the emission profile intensities decrease on adding SM-DNA indicating interaction with DNA. Among ligand **L2**, complex **4** and complex **6**, complex **4** binds strongly to DNA with a sub-micro molar affinity, which shows its potential as anti-cancer agent for in-vitro and in-vivo studies.

Acknowledgement

Lathewdeipor Shadap thanks Dr. Narasinga Palepu Rao for his help, DST-PURSE SCXRD, NEHU-SAIF, Shillong, India for providing Single Crystal X-ray analysis and other spectral studies as well as UGC, New Delhi, India for providing financial assistance in the form of university fellowship (non-Net).

Supplementary material

CCDC 1853646 (**2**), 1853647 (**3**), 1853645 (**4**), 1853642 (**6**), 1853643 (**7**) and 1853644 (**8**) contains the supplementary crystallographic data for this paper. These data can be obtained free of charge via www.ccdc.cam.ac.uk/data_request/cif, by e-mailing data_request@ccdc.cam.ac.uk, or by contacting The Cambridge Crystallographic Data Centre, 12, Union Road, Cambridge CB2 1EZ, UK; Fax: +44 1223 336033.

References

[1] G. Gupta, G.P.A. Yap, B. Therrien, K.M. Rao. Polyhedron 28 (2009) 844.

[2] B. Cornils, W.A. Herrmann, M. Beller, R. Paciello. Applied Homogeneous Catalysis with Organo metallic Compounds. 3RD edition. VCH, Weinheim, 2018.

[3] T. Hirayama, S. Ueda, T. Okada, N. Tsurue, K. Okuda, H. Nagasawa, Chem. Eur. J. 20 (2014) 4156.

[4] V. Niel, A.B. Gaspar, M.C. MuÇoz, B. Abarca, R. Ballesteros, J.A. Real Inorg. Chem. 42 (2003) 4782.

[5] G. Maury, D. Meziane, D. Sraı¨ri, J.P. Paugan, R. Paugam, Bull. Soc. Chim. Belg. 91 (1982) 153.

[6] L.P. Battaglia, M. Carcelli, F. Ferraro, L. Mavilla, C. Pelizzi, G.A. Pelizzi, Dalton Trans. (1994) 2651.

[7] B. Abarca, I. Alkorta, R. Ballesteros, F. Blanco, M. Chadlaoui, J. Elguero and F. Mojarrad Org. Biomol. Chem. 3 (2005) 3905.

[8] J. Klingele, D. Kaase, J. Hilgert, G. Steinfeld, M.H. Klingele, J. Lach Dalton Trans. (2010) 4495.

[9] B. Abarca-Gonzalez, Med. Chem. 17 (2002) 359.

[10] E. Amadei, M. Carcelli, S. Ianelli, P. Cozzini, P. Pelagatti, C. Pelizzi Dalton Trans. (1998) 1025.

[11] P. Sathyadevi, P. Krishnamoorthy, N.S.P. Bhuvanesh, P. Kalaiselvi, V.V. Padma, N. Dharmaraj, Eur. J. Med. Chem. 55 (2012) 420- 431.

[12] T. Nasr, S. Bondock, M. Youns, Eur. J. Med. Chem. 76 (2014) 539-548.

[13] J.M. An, Z.Y. Yang, M.H. Yan, T.R. Li, J. Lumin. 139 (2013) 79-83.

[14] H.Q. Li, L. Cai, J.X. Li, Y.X. Hu, P.P. Zhou, J.M. Zhang, Dyes Pigments 91 (2011) 309-316.

[15] R. Kaplanek, M. Jakubek, J. Rak, Z. Kejik, M. Havlik, B. Dolensky, I. Frydrych, M. Hajduch, M. Kolar, K. Bogdonava, J. Kralova, P. Dzubak, V. Kral, Bioorg. Chem. 60 (2015) 19-29.

[16] M.T. Cocco, C. Congiu, V. Lilliu, V. Onnis, Bioorg. Med. Chem. 14 (2006) 366-372.

[17] V. Judge, B. Narasimhan, M. Ahuja, Med. Chem. Res. 21 (2012) 3940-3957.

[18] D.M. Neumann, A. Cammarata, G. Backes, G.E. Palmer, B.S. Jursic, Bioorg. Med. Chem. 22 (2014) 813.

[19] R. Narang, B. Narasimhan, S. Sharma, Curr. Med. Chem. 19 (2012) 569.

[20] S.M. Sondhi, M. Dinodiaa, A. Kumarb, Bioorganic & Medicinal Chemistry 14 (2006) 4657–4663.

[21] Md. N. Arshad, T.A. Sheikh, Md. M. Rahman, A.M. Asiri, H.M. Marwani, Md.R. Awual, J. Organomet. Chem. 827 (2017) 49-55.

[22] a) G. Jones, Adv. Heterocycl. Chem., 83 (2002) 1–70; b) G. Jones, B. Abarca, Adv. Heterocycl. Chem. 100 (2010) 195 –252.

[23] a) B. Abarca, R. Ballesteros, R. Ballesteros-Garrido, F. Colobert, F. R. Leroux, Tetrahedron 64 (2008) 3794 –3801; b) B. Abarca, R. Ballesteros, F. Blanco, A. Bouillon, V. Collot, J.-R. Domı'nguez, J.-C. Lancelot, S. Rault, Tetrahedron. 60 (2004) 4887 – 4893; c) B. Abarca, R. Ballesteros, M. Chadlaoui, Tetrahedron. 60 (2004) 5785 – 5792; d) B. Abarca, R. Adam, R. Ballesteros, ARKIVOC (2010) 319 –327; e) B. Abarca, R. Adam, R. Ballesteros, L. Chiassai, C. Gamn, ARKIVOC (2012) 229– 241; f) B. Abarca, R. Ballesteros, M. Chadlaoui, J. Miralles, J.V. Murillo, D. Colonna, Tetrahedron. 57 (2001) 10111– 10117; g) B. Abarca-Gonzlez, J. Enzyme Inhib. Med. Chem. 17 (2002) 359– 367.

[24] V. Niel, A.B. Gaspar, M.C. MuÇoz, B. Abarca, R. Ballesteros, J. A. Real, Inorg. Chem. 42 (2003) 4782– 4788.

[25] J. Xiang, Y. G. Yin, P. Mei, Inorg. Chem. Commun. 10 (2007) 1168– 1171;

[26] G. Maury, D. Meziane, D. Sraı¨ri, J.P. Paugan, R. Paugam, Bull. Soc. Chim. Belg. 91 (1982) 153–161.

[27] a) B. Abarca, I. Alkorta, R. Ballesteros, F. Blanco, M. Chadlaoui, J. Elguero, F. Mojarrad, Org. Biomol. Chem. 3 (2005) 3905 –3910; b) J. Klingele, D. Kaase, J. Hilgert, G. Steinfeld, M.H. Klingele, J. Lach, Dalton Trans. 39 (2010) 4495 – 4507; c) E. Escriv, J. Server-Carri, L. Lezama, J.V. Folgado, J.L. Pizarro, R. Ballesteros, B. Abarca, J.

Chem. Soc. Dalton Trans. (1997) 2033 –2038; d) H.E. Zimmerman, A. Ignatchenko, J. Org. Chem. 64 (1999) 6635 – 6645.

[28] a) O. Prakash, H.K. Gujral, N. Rani, S.P. Singh, Synth. Commun. 30 (2000) 417– 425; b) K. Wang, X. Fu, J. Liu, Y. Liang, D. Dong, Org. Lett., 11 (2009) 1015 –1018. (c) J. H. Boyer, R. Borgers, L.T. Wolford, J. Am. Chem. Soc. 79 (1957) 678 – 680.

[29] N.R. Palepu, M.R. Kollipara, J. Chem. Sci. 129 (2017) 177–184.

[30] B. Abarca, R. Ballesteros, M. Chadlaoui, ARKIVOC (vii) (2008) 73-83.

[31] W.L. Armarego, C.L. Chai, (2013) Purification of laboratory chemicals, Butterworth-Heinemann.

[32] M.A. Bennett, T.N. Huang, T. Matheson, A. Smith, S. Ittel, W. Nickerson, Inorg. Synth. 21 (2007) 74.

[33] C. White, A. Yates, P. Maitlis, D. Heinekey, Inorg. Synth. 29 (2007) 228.

[34] Crysalis P R O, release 2012 Version 1.171.36.20. Agilent Technologies, Yarnton.

[35] (a) A. Thorn, B. Dittrich and G.M. Sheldrick, Acta Crystallographica Section A ISSN 0108-7673; (b) George M. Sheldrick, Acta Crystallographica Section A ISSN 2053-2733.

[36] G.M. Sheldrick, Acta Crystallographica Section C: Structural Chemistry Acta. Crystallogr. C 71 **(**2015) 3.

[37] L.J. Farrugia, ORTEP-3 for Windows -a version of ORTEP-III with a Graphical User Interface (GUI). J. Appl. Crystallogr. 30 (1997) 565.

[38] I.J. Bruno, J.C. Cole, P.R. Edgington, M. Kessler, C.F. Macrae, P. McCabe, J. Pearson, R. Taylor, Acta Crystallogr. B 58 (2002) 389- 397.

[39] A.B. Punna Rao, M. Kalidasan, K. Gangele, D.K. Deb, S.L. Shepherd, R. M. Phillips, K. M. Poluri, and M.R. Kollipara. ChemistrySelect 2 (2017) 2065 – 2076.

[40] (a) S.D. Dwivedi, A.K. Singh, S.K. Singh, S. Sharma, M. Chandra, D.S. Pandey, Eur. J. Inorg. Chem., (2008) 5666. (b) K.T. Prasad, B. Therrien, K.M. Rao, J. Organomet.

Chem. 693 (2008) 3049–3056

[41] K.T. Prasad, B. Therrien, K. M. Rao, J. Organomet. Chem. 693 (2008) 3049–3056.

[42] M. Gerloch, E.C. Constable, Transition met. Chem.: the valence shell in d- block chemistry, Wiley Online Library 1994.

[43] A.B.P. Lever, Inorganic electronic spectroscopy, (1968). (b) P. Govindaswamy, Y.A. Mozharivskyj, K.M. Rao, Polyhedron 24 (2005) 1710.

[44] P. Didier, I. Ortmans, A. Kirsch- De Mesmaeker, R. Watts, Inorg. Chem. 32 (1993).

[45] B. Sullivan, D. Salmon, T. Meyer, Inorg. Chem. 17 (1978) 3334- 3341.

[46] K. Jeyalakshmi, J. Haribabu, C. Balachandran, N.S.P. Bhuvanesh, N. Emi, R. Karvembu, New. J. Chem. 41 (2017) 2672.

[47] M.M. Sheeba, M.M. Tamizh, L.J. Farrugia, A. Endo, R. Karvembu, Organomet. 33 (2014) 540.

[48] M. Kalidasan, S.H. Forbes, Y. Mozharivskyj, M.R. Kollipara, Inorg. Chim. Acta 421 (2014) 218.

[49] Y. Hanifehpour, B. Mirtamizdoust, S.W. Joo, J. Inorg. Organomet. Polym. 22 (2012) 916.

[50] R. Payne, P. Govender, B. Therrien, C.M. Clavel, P.J. Dyson, G.S. Smith, J. Organomet. Chem. 729 (2013) 20.

[51] M.A. Jakupec, M. Galanski, V.B. Arion, C.G. Hartinger, B.K. Keppler, Antitumour metal compounds: more than theme and variations, Dalton Trans. 2 (2008) 183–194.

[52] P.J. Dyson, G. Sava, Metal-based antitumour drugs in the post genomic area, Dalton Trans. (2006) 1929–1933.

[53] Synthesis, characterization, DNA binding, DNA cleavage, protein binding and cytotoxic activities of Ru(II) complexes. S. Thota et al. / International Journal of Biological Macromolecules 82 (2016) 663–670.

[54] K.J. Du, J.Q. Wang, J.F. Kou, G.Y. Li, L.L. Wang, H. Chao, L.N. Ji, Synthesis, DNA binding and topoisomerase inhibitory activity of ruthenium(II) polypyridyl complexes, Eur. J. Med. Chem. 46 (2011) 1056–1065.

[55] J.F. Kou, C. Qian, J.Q. Wang, X. Chen, L.L. Wang, H. Chao, L.N. Ji, Chiral ruthenium(II) anthroquinone complexes as dual inhibitors of topoisomerses I and II, J. Biol. Inorg. Chem. 17 (2012) 81–96.

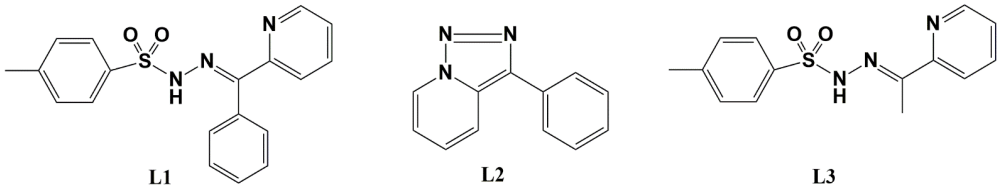

Chart **1:** Ligands used in study

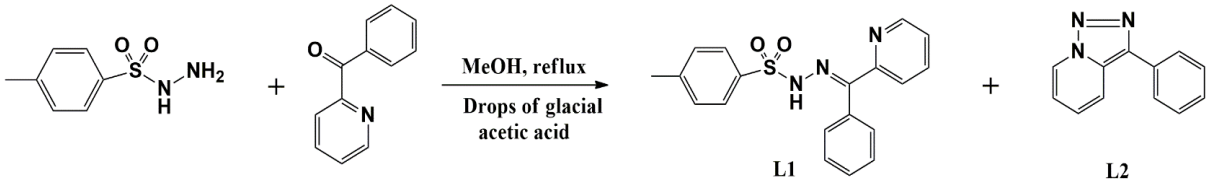

Scheme **1**: Preparation of ligands (**L1** and **L2**)

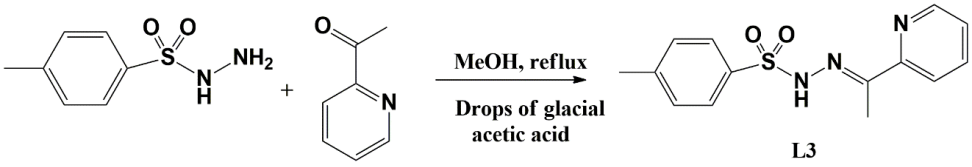

Scheme **2**: Preparation of ligand (**L3**)

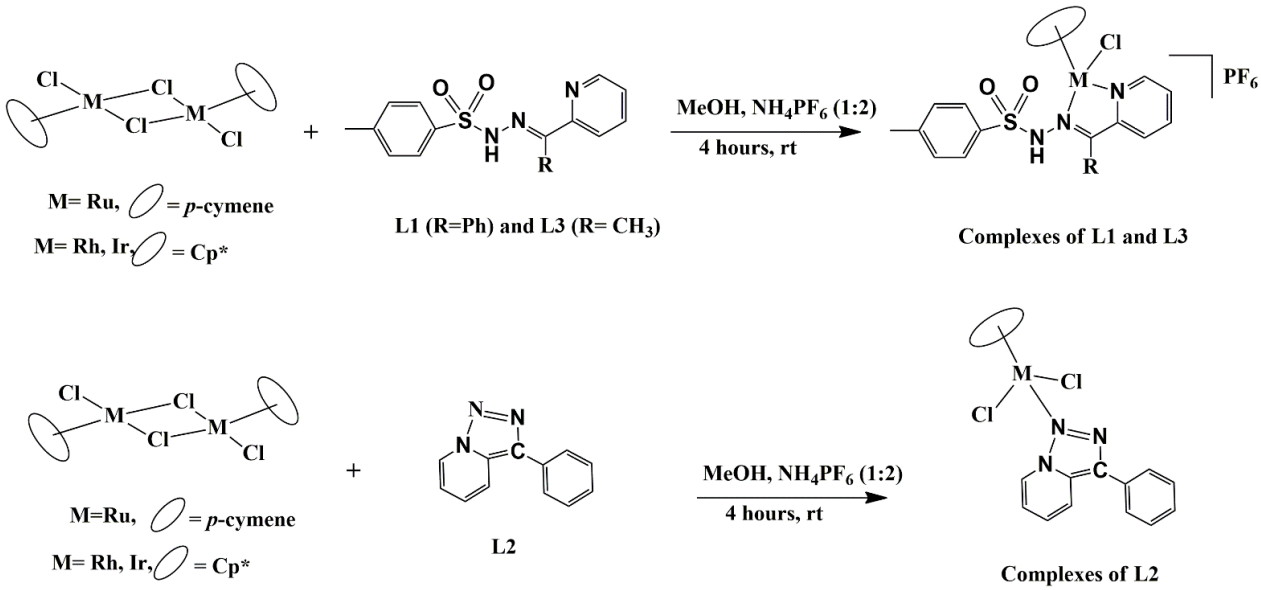

Scheme **3**: Preparation of complexes.

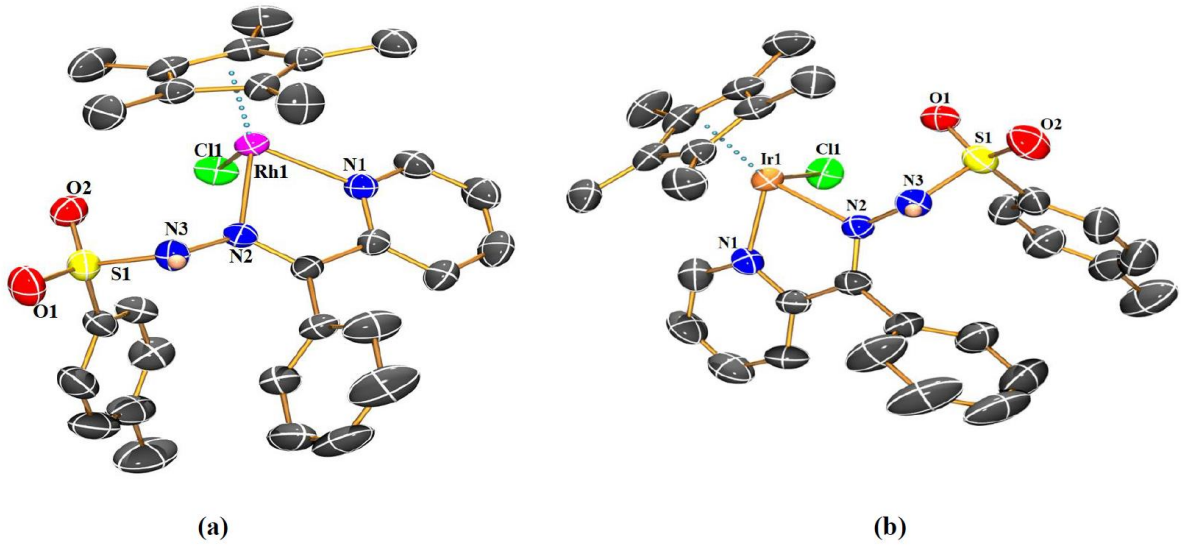

Figure 1: (a) ORTEP diagram of complex (**2**) and (b) ORTEP diagram of complex (**3**) with 50% probability thermal ellipsoids. Hydrogen atoms and counter ions have been omitted for clarity.

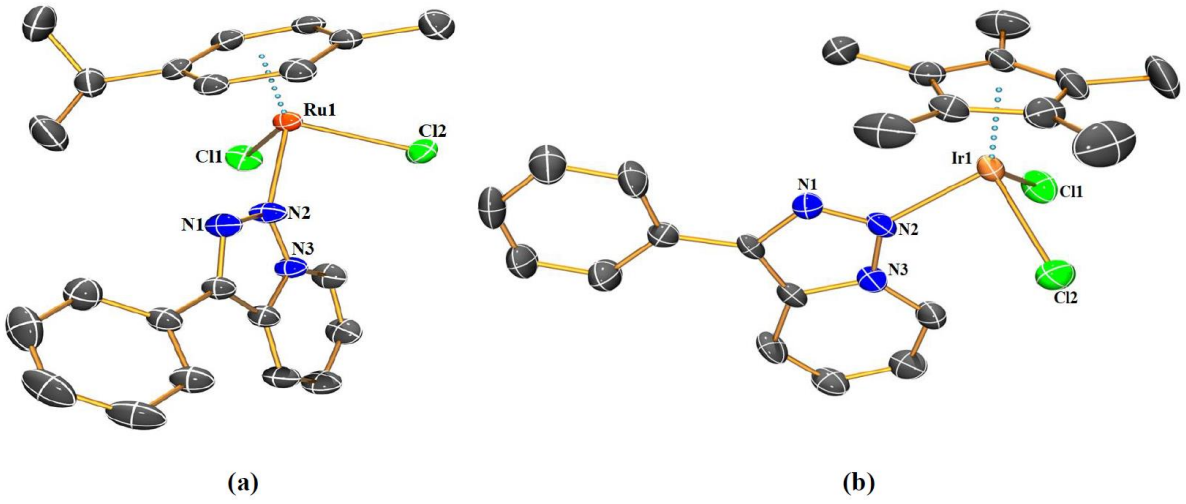

Figure 2: (a) ORTEP diagram of complex (**4**) and (b) ORTEP diagram of complex (**6**) with 50% probability thermal ellipsoids. Hydrogen atoms, counter ions and residual metal precursor (in case of complex **6**) have been omitted for clarity.

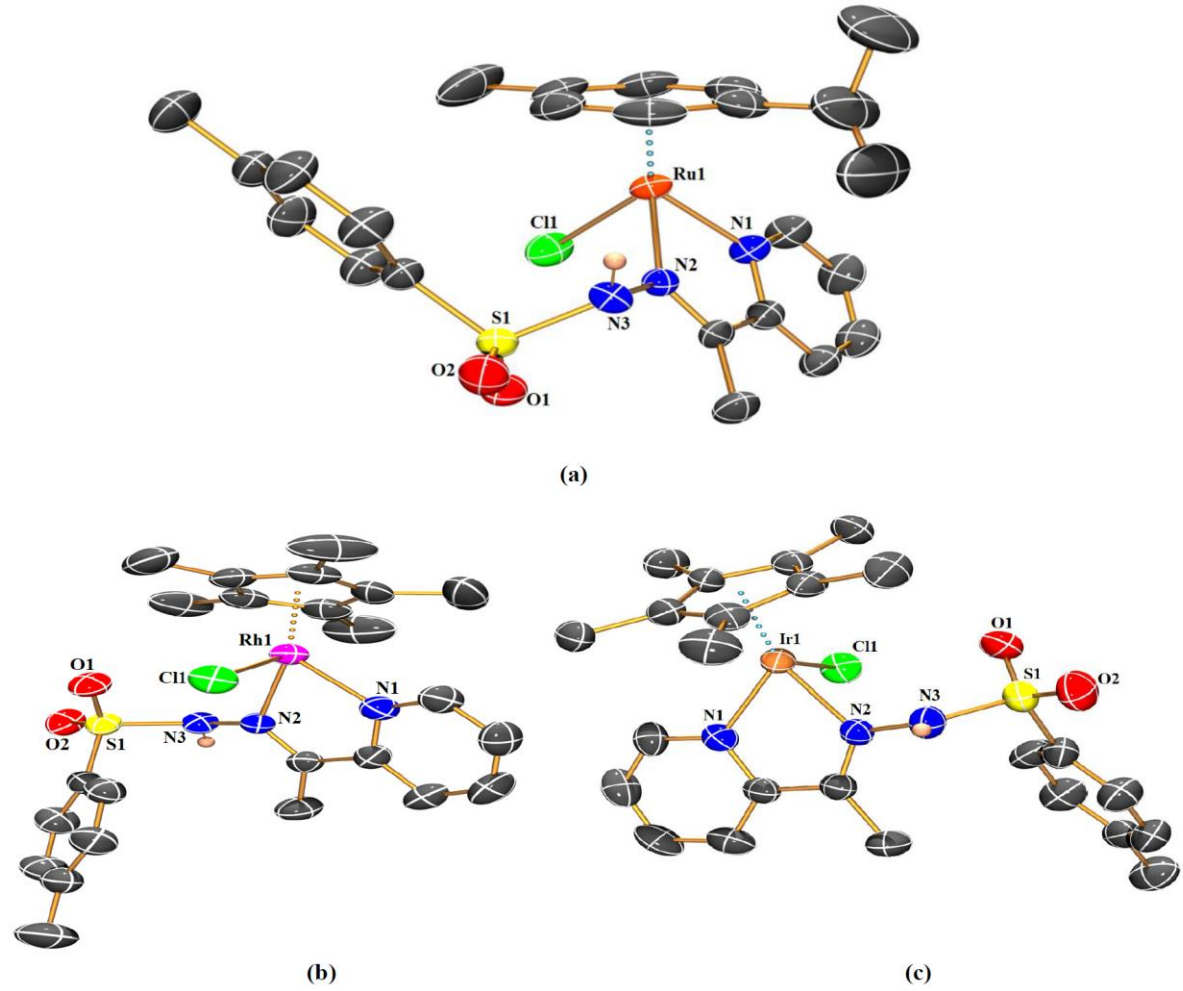

Figure 3: (a) ORTEP diagram of complex (**7**) and (b) ORTEP diagram of complex (**8**) (c) ORTEP diagram of complex (**9**) with 50% probability thermal ellipsoids. Solvent molecules, counter ions and hydrogen atoms are omitted for clarity. ORTEP diagram of Complex **9** has just been given to shown the mode of binding and composition of the complex.

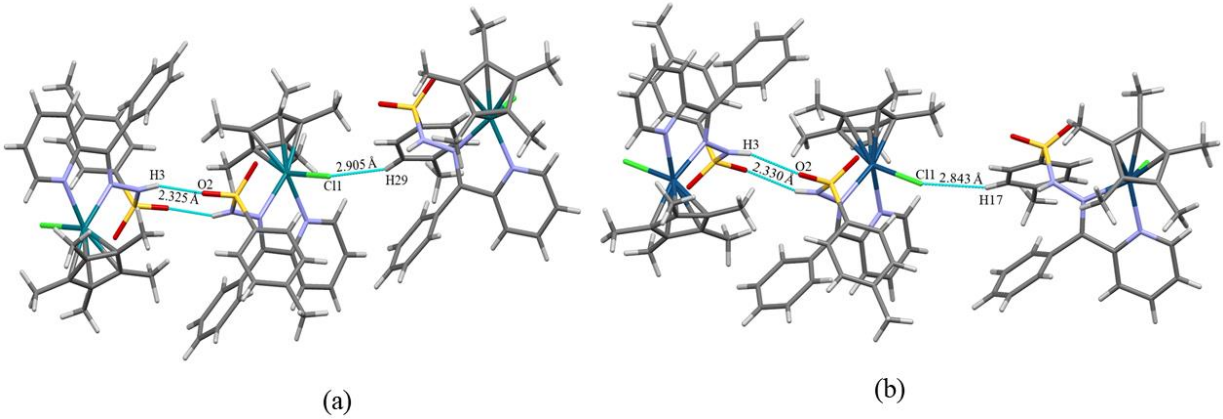

Figure 4: (a) Complex **2** showing inter hydrogen bonding O(2)---(3)H and H(29)---Cl(1) (b) complex **3** showing inter hydrogen bonding O(2)---(3)H and H(17)---Cl(1).

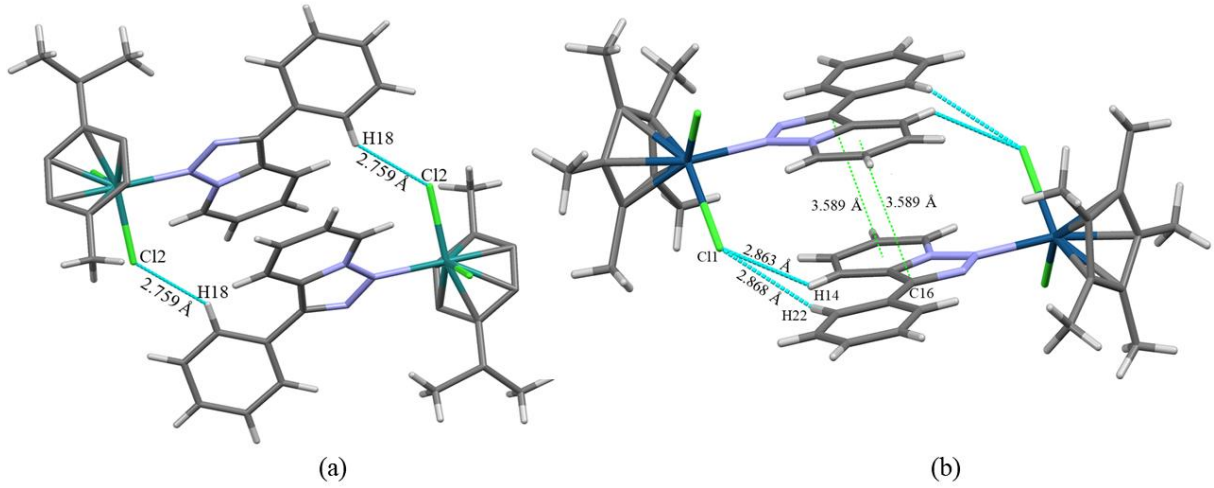

Figure 5: (a) Complex **4** showing inter hydrogen bonding H(18)---Cl(2) and (b) Complex **6** showing inter hydrogen bonding H(14)---Cl(1) and H(22)---Cl(1) and C---π interactions.

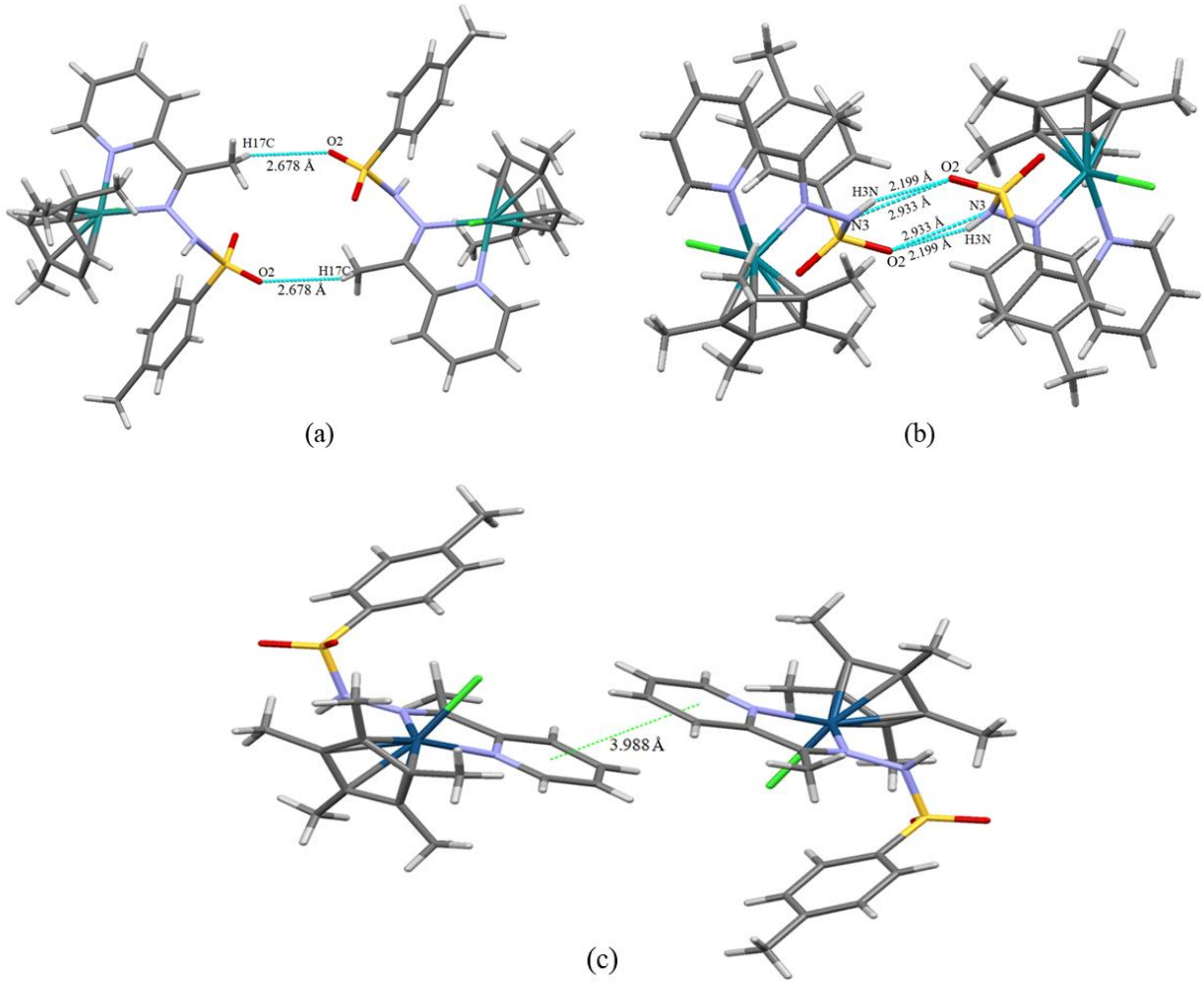

Figure 6: (a) Complex **7** showing inter hydrogen bonding H(17C)---O(2), (b) Complex **8** showing inter hydrogen bonding O(2)---H(3N) and covalent interaction O(2)---N(3) (c) Complex **9** showing π---π interaction.

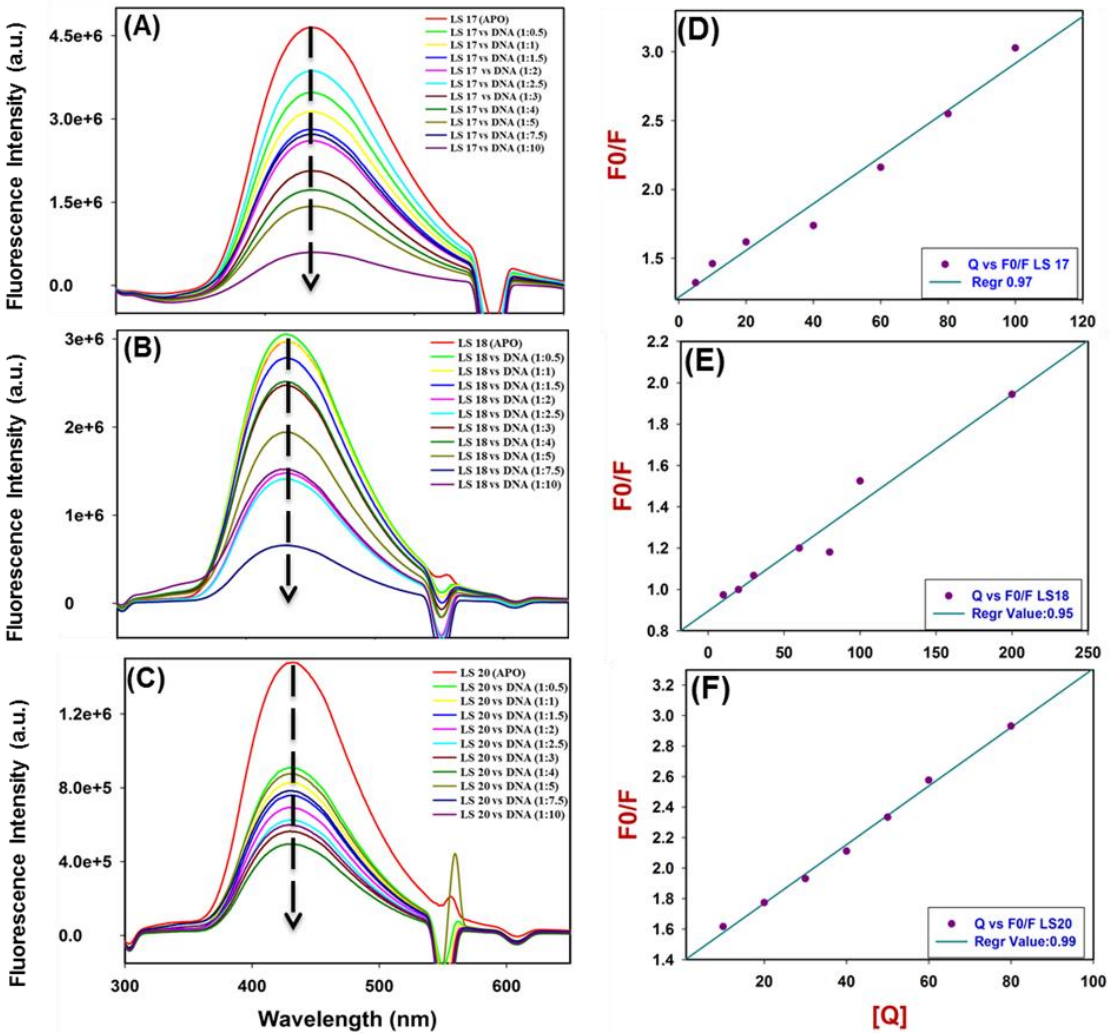

Figure 7: (A-C): The emission profile (λ_{ex}= 275 nm; λ_{em}= 300-650 nm) of ligand (L2) **(A)**, complex 4 **(B),** and complex 6 **(C)** at 20 µM in the presence of increasing concentrations of SM-DNA (10 µM-200 µM). The arrows represent the changes in emission intensity upon addition of SM DNA. **D-F** represents F0/F vs [Q] plots for complexes ligand (L2), complex 4 and complex 6 respectively.

Table 1: Crystal structure data and refinement of complexes **2, 3** and **4**.

Complexes	[**2**]PF_6	**[3]**PF_6	[**4**]
Empirical formula	$C_{29}H_{32}ClF_6N_3O_2PRhS$	$C_{29}H_{32}ClF_6IrN_3O_2PS$	$C_{22}H_{23}Cl_2N_3Ru$
Formula weight	769.96	859.25	501.40
Temperature (K)	293(2) K	292.2(7)	292(2)
Wavelength (Å)	0.71073	0.71073	0.71073
Crystal system	monoclinic	monoclinic	triclinic
Space group	*P 21/c*	*P 21/c*	*P -1*
a (Å)/α (°)	14.3284(9)/90	14.4592(6)/90	7.6746(6)/93.200(6)
b (Å)/β (°)	15.8911(13)/115.152(7)	15.5533(5)/115.559(5)	10.1164(8)/90.474(7)
c (Å)/γ (°)	15.6936(9)/90	15.7417(6)/90	13.8190(11)/105.681(7)
Volume ($Å^3$)	3234.5(4)	3193.7(2)	1031.05(15)
Z	4	4	2
Density (calc) (Mg/m^{-3})	1.581	1.787	1.615
Absorption coefficient (μ) (mm^{-1})	0.791	4.447	1.032
F(000)	1560	1688	508
Crystal size (mm^3)	0.29 x 0.25 x 0.12	0.21 x 0.15 x 0.11	0.25 x 0.13 x 0.12
Theta range for data collection	3.393 to 28.844	3.123 to 25.349	3.160 to 29.120
Index ranges	-17<=h<=18, -20<=k<=20, -20<=l<=20	-17<=h<=16, -13<=k<=18, -18<=l<=14	-10<=h<=7, -12<=k<=13, -18<=l<=18
Reflections collected	13016	11735	7016
Independent reflections	7315 [R(int) = 0.0355]	5811 [R(int) = 0.0312]	4652 [R(int) = 0.0363]
Completeness to theta = 25.00°	99.5	99.4	99.1
Absorption correction	Semi-empirical from equivalents	Semi-empirical from equivalents	Semi-empirical from equivalents
Refinement method	Full-matrix least-squares on F^2	Full-matrix least-squares on F^2	Full-matrix least-squares on F^2
Data/restraints/parameters	7315/93/461	5811/93/442	4652/ 0/256
Goodness-of-fit on F_2	1.063	1.052	1.008
Final R indices [I>2sigma(I)]	R1 = 0.0551, wR2 = 0.1053	R1 = 0.0339, wR2 = 0.0769	R1 = 0.0319, wR2 = 0.0688
R indices (all data)	R1 = 0.0844, wR2 =0.1196	R1 = 0.0496, wR2 = 0.0861	R1 = 0.0377, wR2 = 0.0710
Largest diff. peak and hole($e.Å^{-3}$)	1.046 and -0.5538	1.094 and -1.097	0.528 and -0.793
CCDC No.	1853646	1853647	1853645

Table 2: Crystal structure data and refinement of complexes **6, 7** and **8**.

Complexes	[**6**]	[**7**]PF_6	**[8]**PF_6
Empirical formula	$C_{32}H_{39}Cl_4Ir_2\ N_3$	$C_{24}H_{29}ClN_3O_2RuSF_6P$	$C_{24}H_{30}ClN_3O_2RhSF_6PCH_2Cl_2$
Formula weight	991.86	705.05	792.82
Temperature (K)	296.0(4)	294(2)	293(2) K
Wavelength (Å)	0.71073	0.71073	0.71073 Å
Crystal system	monoclinic	triclinic	Monoclinic
Space group	*I 2/a*	*P -1*	*P 21/n*
a (Å)/α (°)	17.7774(8)/90	10.6281(5)/85.109(4	14.9319(6)/90
b (Å)/β (°)	8.6283(3)/94.451(4)	11.2246(5)/79.880(4)	14.2711(5)/113.732(5)
c (Å)/γ (°)	43.0393(14)/ 90	12.6687(6)/75.358(4)	16.6130(7)/90
Volume ($Å^3$)	6581.8(4)	1438.17(12)	3240.8(2)
Z	8	2	4
Density (calc) (Mg/m^{-3})	2.002	1.628	1.625
Absorption coefficient (μ) (mm^{-1})	8.431	0.833	0.951
F(000)	3792	712	1600
Crystal size (mm^3)	0.25 x 0.23 x 0.21	0.3 x 0.2 x 0.16	0.250 x 0.230 x 0.210
Theta range for data collection	3.8090 to 28.7880	2 to 20	3.221 to 28.962
Index ranges	-24<=h<=13, -11<=k<=10, -58<=l<=52	-13<=h<=10, -15<=k<=14, -14<=l<=16	-20<=h<=11, -19<=k<=18, -12<=l<=21
Reflections collected	13730	9988	14228
Independent reflections	7546 [R(int) = 0.0326]	6439 [R(int) = 0.0319]	7475 [R(int) = 0.0272]
Completeness to theta = 25.00°	99.4	99.01	99.5
Absorption correction	Semi-empirical from equivalents	Semi-empirical from equivalents	Semi-empirical from equivalents
Refinement method	Full-matrix least-squares on F^2	Full-matrix least-squares on F^2	Full-matrix least-squares on F^2
Data/restraints/parameters	7546/0/380	6439/ 0/361	7475 / 63 / 469
Goodness-of-fit on F_2	1.009	1.041	1.044
Final R indices [I>2sigma(I)]	R1 = 0.0351, wR2 = 0.0521	R1 = 0.0474, wR2 = 0.1096	R1 = 0.0458, wR2 = 0.1007
R indices (all data)	R1 = 0.0500, wR2 = 0.0562	R1 = 0.0589, wR2 = 0.1172	R1 = 0.0685, wR2 = 0.1130
Largest diff. peak and hole($e.Å^{-3}$)	0.930 and -1.139	0.623 and -0.629	0.729 and -0.555
CCDC No.	1853642	1853643	1853644

Table 3. Selected bond lengths (Å) and bond angles (°) of complexes **2, 3, 7,** and **8**.

Complexes	**2**	**3**	**7**	**8**
M-CNT	1.795	1.798	1.703	1.785
M(1)-N(1)	2.111(3)	2.094(4)	2.081(3)	2.084(3)
M(1)-N(2)	2.158(3)	2.115(4)	2.091(3)	2.132(3)
M(1)-Cl(1)	2.4183(11)	2.4007(14)	2.3898(10)	2.4087(9)
N(1)-M(1)-N(2)	75.14(12)	75.16(16)	75.58(11)	75.24(11)
N(1)-M(1)-Cl(1)	84.79(10)	83.34(13)	81.69(9)	84.12(8)
N(2)-M(1)-Cl(1)	95.42(9)	93.06(12)	87.55(7)	93.60(7)

CNT represents the centroid of the arene/Cp* ring and (M = Ru, Rh and Ir)

Table 4. Selected bond lengths (Å) and bond angles (°) of complexes **4** and **6.**

Complexes	**4**	**6**
M-CNT	1.795	1.798
M(1)-N(2)	2.1482(19)	2.155(4)
M(1)-Cl(2)	2.4277(6)	2.4126(14)
M(1)-Cl(1)	2.4235(7)	2.4128(14)
N(2)-M(1)-Cl(1)	86.34(6)	87.19(12)
Cl(1)-M(1)-Cl(2)	88.95(2)	88.80(5)
N(2)-M(1)-Cl(2)	88.24(6)	90.52(12)

Table 5: Binding constant for the interaction of complexes with SM-DNA.

Compound	Quenching Constant (Kq) m^{-1} s^{-1}	Dissociation Constant (Kd) [M]
Ligand (L2)	$3.7x10^{12}$	$8.1x10^{-4}$
Complex 4	$1.9x10^{12}$	$1.0x\ 10^{-7}$
Complex 6	$6.1x10^{12}$	$3x10^{-3}$

HIGHLIGHTS

- Triazolo derivatives *i.e* L2, 4 and 6 showed high potency towards DNA binding
- L1 and L3 formed cationic complexes while L2 ligand formed neutral complexes.
- The complexes showed intermolecular hydrogen bonding and weak covalent interactions.